

## New Experimental Technique for Dynamic Bending of Composite Materials

*The paper is dedicated to our colleague and friend Prof. Piotr Perzyna  
from IPPT who passed away on June 22, 2013*

Abdellah MASSAQ<sup>1),2)</sup>, Alexis RUSINEK<sup>3)</sup>, Maciej KLÓSAK<sup>4)</sup>

<sup>1)</sup> *Ecole Nationale des Sciences Appliquées*  
BP575, Avenue Abdelkrim Khattabi, 40000, Guéliz-Marrakech, Morocco

<sup>2)</sup> *Ibn Zohr University – Faculty of Sciences Agadir*  
BP. 8106 Quartier Dakhla, Agadir, Morocco  
e-mail: a.massaq@uiz.ac.ma

<sup>3)</sup> *National Engineering School of Metz ENIM*  
*Laboratory of Mechanics, Biomechanics, Polymers and Structures – LaBPS, EA 4632*  
1 route d’Ars Laquenexy, CS 65820 57078 METZ Cedex 3, France  
e-mail: rusinek@enim.fr

<sup>4)</sup> *Universiapolis, Ecole Polytechnique d’Agadir*  
Bab Al Madina, Quartier Tilila, Agadir, Morocco  
e-mail: klosak@e-polytechnique.ma

The paper is reporting a new experimental technique to study the dynamic behaviour of composite materials subjected to bending direct impact. It is based on the Hopkinson bar system allowing to observe material behaviour at very high impact velocities. The material used to perform the tests is a woven glass-fibre-reinforced Polyamide 6.

**Key words:** impact velocity, dynamic bending, composite, shock, Hopkinson bar.

### 1. INTRODUCTION

The interest in bending tests results from the simplicity of specimen geometry and their popularity in industry. The composite material properties given by quasi-static bending tests are most popular. However, the bending load of a specimen and the result analysis is not simple. It remains very complex and yet many

authors use this test as an easy and reliable tool. This happens generally due to the low cost of this method. As far as dynamic bending tests are concerned, they are used for toughness measurements [1]. Usual bending tests with a shock impact at the notched specimens are performed on the Charpy apparatus [2, 3]. A load-time curve registered during the test using gauges installed on a projectile or on supports, reveals many important oscillations. These oscillations make it quite difficult to interpret the results. In fact, the obtained signal is a complex combination of the specimen response, the inertial loading of specimen acceleration, the direction of tension and compression waves in both, the specimen and the projectile. As a matter of fact, the projectile is subjected to elastic waves propagation which make the results difficult to exploit. If the material is fragile, the specimen rupture may appear during first oscillations, even at a inertial peak, so it is easy to guess areliable result analysis is hardly possible. In general, dynamic bending cannot provide a reliable information on a rupture from force measurements. Bending waves are relatively slow and specimen vibrations generate a lot of perturbations. The use of Hopkinson bar [4] helps to eliminate some of those problems and to obtain a better quality of the results.

A 3-point bending test on the Hopkinson bar has several advantages. It is relatively simple and not expensive to determine the applied load as well as the deflection of the specimen. However, when used in a classical manner, restrictions are imposed on the projectile type and the test time, because no waves superposition may occur at the level where gauges are installed.

In order to answer these questions and also other ones that will be discussed further, we propose a new experimental technique based on the Hopkinson bar system in order to measure displacements in the middle of the specimen and to obtain high impact velocities. In this study, we will examine the behaviour of the woven glass-fibre-reinforced Polyamide 6 submitted to dynamic bending.

## 2. EXPERIMENTAL TECHNIQUES AND MEASUREMENTS

The technique that has been developed during this study is based on the principle of the 3-point bending on the Hopkinson bar.

In order to evaluate the resistance to the dynamic rupture of materials with energy stored in the specimen, many authors [5, 6] have used the Hopkinson bars for the 3-point bending tests (Fig. 1).

This calculation requires that the applied load as well as the displacement at mid-span of the specimen are known. The rupture shall occur before the wave performs back-and-forth in the projectile and also before incident and reflection waves are superposed. We will not be able to separate these waves by using the classical method. In the presented study, the support deformation is not

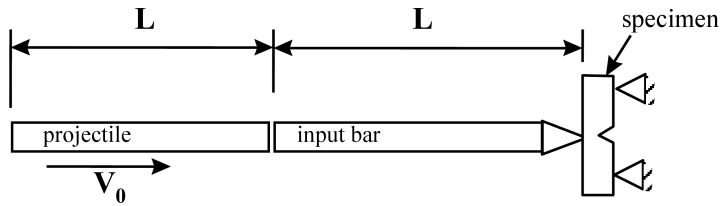


FIG. 1. Bending test using the Hopkinson bar system, without output bar.

taken into account. In return, two output bars have been added to cover this inconvenience.

The most frequent arrangement for the Hopkinson 3-point bending test consists of two output bars [7-13] which enables to determine reactions at the support level (Fig. 2). The loading is applied through the input bar. It should be noted that certain authors [7, 8] do not exploit a simple advantage that a displacement of the specimen can easily be calculated.

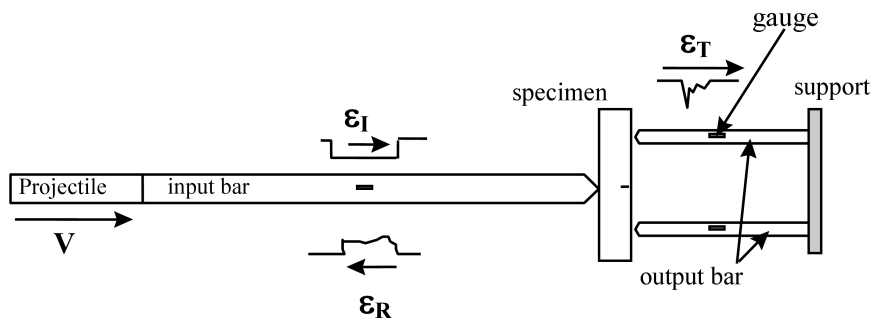


FIG. 2. Bending test using the Hopkinson bar system with two output bars.

A special conic shaped projectile (Fig. 3) is proposed in order to avoid problems with perturbations caused by the impedance variations during the indirect impact. It means the input bar is suppressed and the projectile enters into direct contact with the specimen (Fig. 4). The measurements of the displacement during the time are made with an optical extensometer type Zimmer which follows

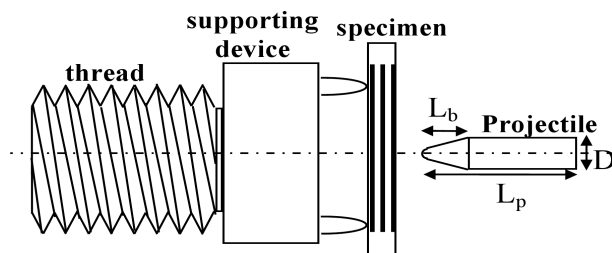


FIG. 3. Geometry of the projectile and device to fix the specimen.

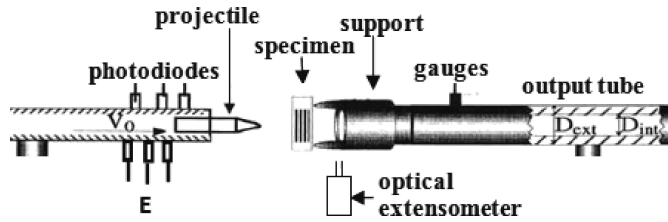


FIG. 4. Modified configuration for dynamic 3 points bending test.

the movement of the specimen without contact. The extensometer reacts to the axial displacement of small black and white target glued at the central part of the tensile face of the specimen. The projectile velocity is measured by using a system of three sources of light and photodiodes linked to two time counters. The knowledge of the velocity at these two point enables to calculate an average velocity of the projectile just before impact.

In order to minimize the Pochhammer-Chree type vibration, which is registered during the impact at the bar end [14], two output bars have been replaced by a tube (Fig. 4). The radial inertia is by far smaller in the tube than in the plain bar in the case of the same external geometry [15, 16]. The radial dispersion is then split into external and internal ones.

The specimen is attached to the supporting devise produced of a thermally treated steel. This supporting device can be easily installed and uninstalled as it has a special thread (Fig. 3). The supporting device protects the tube, so the latter will not require any treatment in case of damage. A schematic demonstration of this assembly is shown in Fig. 4.

The gauges are glued on the output bar, therefore the signal of the transmitted axial force applied to the specimen can be read from the wave of the transmitted longitudinal deformation  $\varepsilon_T(t)$ . The extremity of the projectile has a bevelled form of the length  $L_b$  and the projectile length is  $L_p$ . The assembly characteristics are given in Table 1. Figure 5 illustrates the Lagrange diagram for the studied dynamic bending configuration using a short projectile.

**Table 1.** Characteristics of the projectile and the tube.

Projectile length of the projectile	$L_p = 100$ mm
Length of the conic part of the projectile	$L_b = 30$ mm
Projectile diameter	$D = 22$ mm
Projectile mass	$m = 215$ g
Tube length	$L_h = 4000$ mm
Internal diameter of the tube	$D_{\text{int}} = 30$ mm
External diameter of the tube	$D_{\text{ext}} = 50$ mm

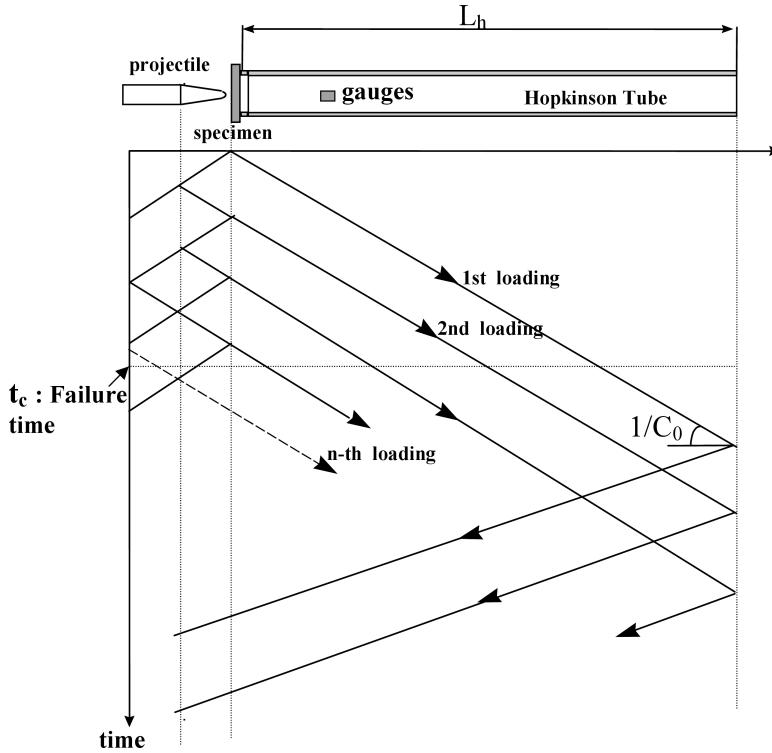


FIG. 5. Lagrange diagram for dynamic bending test.

As far as the modified version of the 3-point Hopkinson bending is concerned, there are some important advantages of this configuration, mainly:

- impact velocities may reach up to 200 m/s, whereas the Charpy test is limited to 5 m/s,
- the loading by impact eliminates the rise time between the incident wave in the bar and the transmitted wave in the output tube,
- a reduction in the apparatus dimensions.

The axial force transmitted through the specimen to the supports can be determined as a function of time of the transmitted longitudinal wave  $\varepsilon_T(t)$ . It is measured using two deformation gauges attached to the tube at two opposite extremities in order to eliminate the impact of the tube bending. The support reaction can be therefore given by:

$$(2.1) \quad F(t) = \frac{\pi}{4} (D_{\text{ext}}^2 - D_{\text{int}}^2) \cdot E_{\text{tub}} \cdot \varepsilon_T(t),$$

where  $E_{\text{tub}}$  is the Young's modulus of the tube,  $D_{\text{ext}}$  and  $D_{\text{int}}$  are, respectively, the external and internal diameters of the Hopkinson tube.

The real displacement of the central point of the tensile face of the specimen  $\delta_s$  imposed by the projectile can be expressed by:

$$(2.2) \quad \delta_s(t) = \delta_{\text{ext}}(t) - \delta_{\text{tub}}(t),$$

where  $\delta_{\text{ext}}$  and  $\delta_{\text{tub}}$  represent, respectively, the displacement measured as tension by the optical extensometer and by the gauges placed at the Hopkinson bar. An analysis of the elastic wave propagation allows to determine the tube displacement as a function of the transmitted wave  $\varepsilon_T(t)$ . The value of  $\delta_{\text{tub}}$  can be expressed as following:

$$(2.3) \quad \delta_{\text{tub}}(t) = c_0 \int_0^t \varepsilon_T(\xi) d\xi.$$

The combination of the Eqs. (2.2) and (2.3) gives a real displacement in the middle of the specimen:

$$(2.4) \quad \delta_s(t) = \delta_{\text{ext}}(t) - c_0 \int_0^t \varepsilon_T(\xi) d\xi.$$

The graphical characteristics of the signals measured by the gauges and the extensometers are presented in Fig. 6. They have been obtained during the

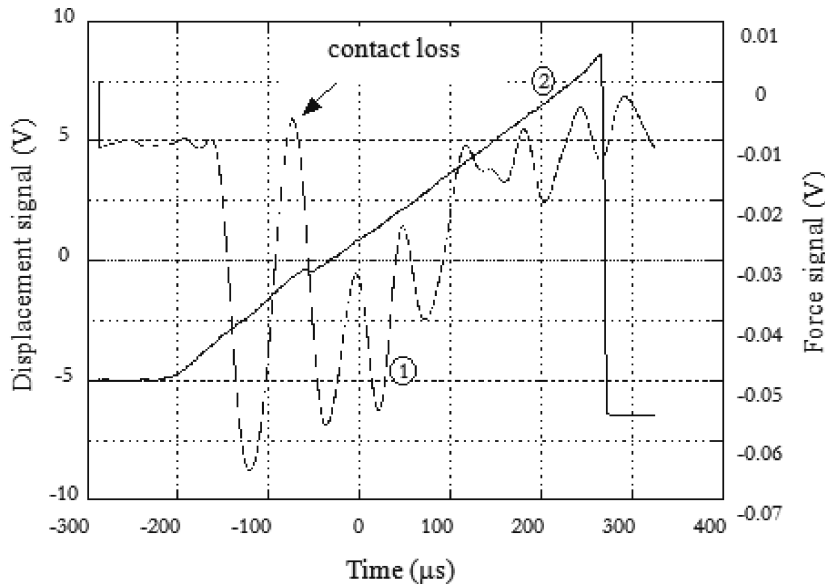


FIG. 6. Graphical presentation of displacement (2) and force (1).

test with the impact loading of 17 m/s. It can be seen the signal registered by the gauges attached to the transmitted bar has many oscillations. We can also observe a loss of contact between the specimen and the supports during 85  $\mu$ s after impact. That means the specimen remains without any contact with the supports during 36  $\mu$ s (Fig. 6). It clearly demonstrates the complexity of this phenomenon compared to a simple 3-point bending under quasi-static loading. It is therefore very important to give the physical meaning for this behaviour.

### 3. STUDY IN THE WOVEN GLASS-FIBRE-REINFORCED POLYAMIDE 6 UNDER DYNAMIC BENDING

#### 3.1. Material

The tested material is a composite reinforced by the glass fibre with a matrix of Polyamide 6 (PA6). Our tests have been performed using parallelepiped specimens without notches, cut from one plate of the glass-fibre-reinforced PA6 with identical characteristics in length, width and slenderness ratio. The specimen geometry is presented in Fig. 7 and it resembles the Charpy's geometry as its width  $S$  between two supports is equal to 40 mm [17]. In order to diminish a negative effect of inertial forces on the transmitted force at high impact velocities, we have adopted a configuration defined by the  $S/W$  ratio of the order of 4.5. Both superior and inferior faces are not treated in order not to disturb existing surface imperfections.

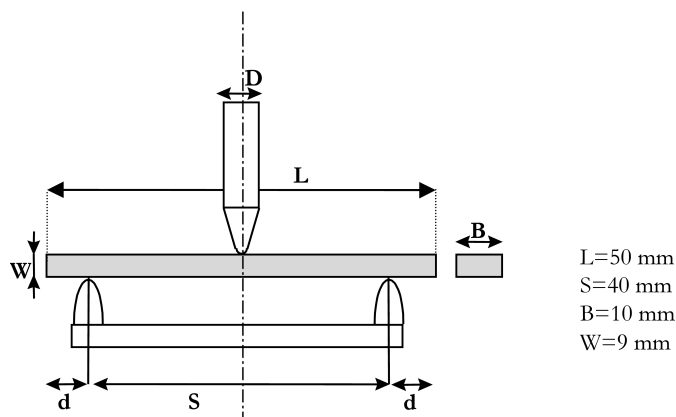


FIG. 7. Geometry of the Charpy specimen loaded by the Hopkinson bar.

#### 3.2. Analysis and discussion

Figures 8 and 9 represent the evolution of the transmitted force and of the displacement as a function of time. It can be observed that the increasing phase

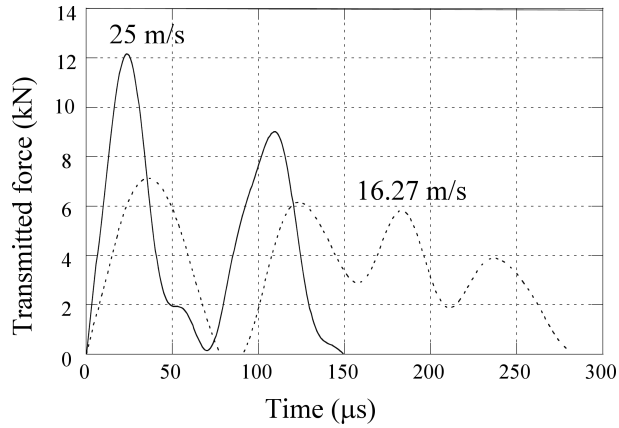


FIG. 8. Evolution of the force measured as a function of time.

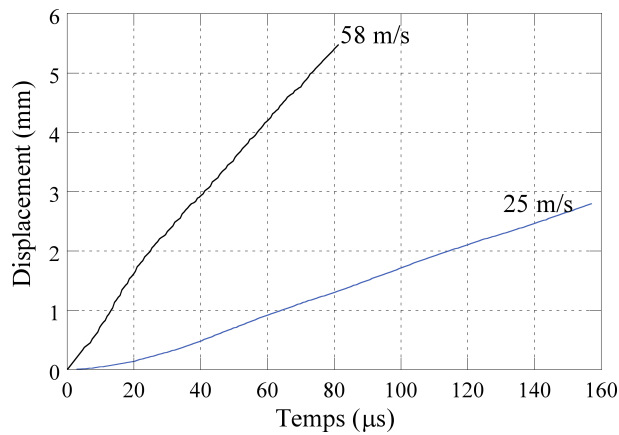


FIG. 9. Evolution of the measured displacement versus time.

of the force is relatively short, of the order of 20–35  $\mu\text{s}$ . The loading phase is accompanied by one or more oscillations of the variable amplitude. On the other hand, the variation of displacement measured as function of time, using a Zimmer sensor displacement without contact, is quasi linear. The displacement evolution as a function of time stops just after the last peak of the force-time curve, this point being translated as the rupture point of the specimen. In fact, the velocity of the mid-point of the specimen is quasi-constant.

The first force peak reflects a start of the specimen solicitation. Its high amplitude compared to other amplitudes can be simply explained by a high value of the force generated by the inertia of the specimen at the beginning of the velocity increase. Then, it can be stated the force not only comes to zero, but it takes a negative value during a short period of time. This is explained

by the loss of contact between the specimen and the supports. The contact is re-established during the second loading. It can be deduced the projectile has a slightly lower velocity than the central point of the specimen. The rupture occurs principally in the form of “one point bending” where the only resistance of the specimen is due to its inertia.

The importance of oscillations in the signal of the support reactions made us analyze more attentively the behaviour of an isotropic bar in the vibration mode and subjected to the 3-point bending. First, the vibration modes have been evaluated analytically.

### 3.3. Study of the beam behaviour

During the first instants when the deformation wave arrives at the interface projectile-specimen, the wave in the specimen do not still reach the supports and the test remains equivalent to the test of “one point bending”. As a consequence, it is proposed to adopt a semi-infinite beam to model the specimen. The movement equation  $Y(z, t)$  of the beam in bending, for which only the effects of the bending moment are considered, can be expressed by:

$$(3.1) \quad \frac{\partial^4 Y}{\partial z^4} + 4\alpha^4 \frac{\partial^2 Y}{\partial t^2} = 0 \quad \text{where} \quad 4\alpha^2 = \frac{\rho S}{EI},$$

where  $E$  is the Young's modulus of the material,  $\rho$  is the density;  $I$  and  $A$  are respectively the quadratic moment  $I = \frac{BW^3}{12}$  and the specimen cross-section  $A = BW$ ;  $Y(z, t)$  is the beam deformation. More information are reported in Appendix.

The resolution of this equation is a proper pulsation of the  $n$ -mode of the free frequency [18] (for details see Appendix):

$$(3.2) \quad \omega_n = n^2 \pi^2 \sqrt{\frac{EI}{\rho AS^4}} = n^2 \pi^2 \sqrt{\frac{EI}{m_0 S^3}},$$

where  $S$  is the distance between the supports and  $m_0 = \rho AS$  corresponds to the mass between the specimen supports.

The frequency is given by the following formula:

$$(3.3) \quad y_n(z) = y_0 \sin\left(\frac{n\pi z}{S}\right),$$

where  $y_0$  is a constant.

The deformed shape of the first five resonant frequencies is schematized in Fig. 10. The corresponding values of pulsations for the glass-fibre-reinforced Polyamide 6 specimen are reported in Table 2.

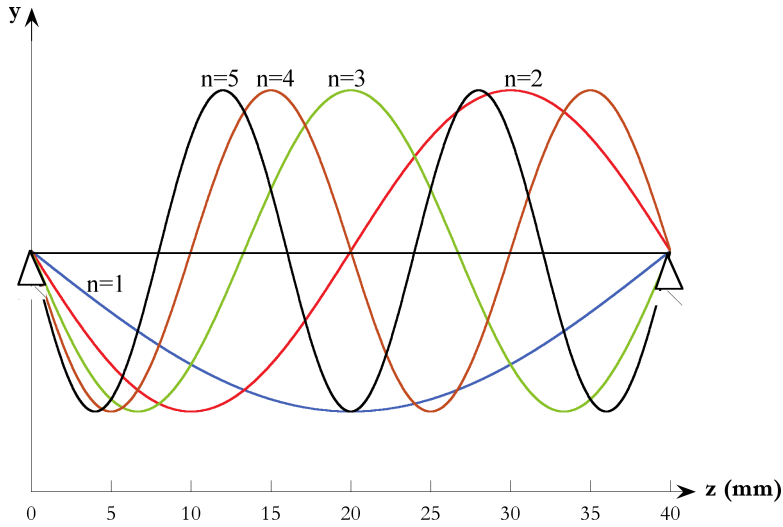


FIG. 10. Shape of first five resonant frequencies of the beam in bending.

**Table 2.** Pulsations values and periods of first five resonant frequencies.

$n$	1	2	3	4	5
$\omega_n$ (rd/s)	$27.2 \cdot 10^3$	$108.6 \cdot 10^3$	$244.4 \cdot 10^3$	$434.4 \cdot 10^3$	$678.8 \cdot 10^3$
$T_n$ ( $\mu$ s)	231	58	26	14.4	9.3

When a cantilever shape of the specimen is taken into account, i.e. we include the parts of the specimen which extends beyond the supports, the value of the proper pulsations is modified (Fig. 7). This correction corresponds to the cantilever  $p = (L - S)/2S = 0.125$ . This value leads to the diminution of the first mode pulsation to 22.345 rd/s. The ratio  $\omega_n/\omega_n^\circ$  corresponds to the value of 0.823, where  $\omega_n^\circ$  is linked to the  $n$ -th proper mode defined by the relation (3.2).

The oscillations period  $\omega$  has been determined graphically from the oscillations observed at the force-time curves. The results grouped at Fig. 11 present the mean pulsations values obtained at different impact velocities. It can be noted this pulsation seems to vary linearly as a function of  $\log(V_i)$ . A linear correlation leads to the following equation:

$$(3.4) \quad \omega = \omega_0 + \beta \log(V_i/V_0),$$

$V_i$  is the impact velocity.

For  $V_0 = 1$  m/s, the pulsation at the low velocity is  $\omega_0 = 42323$  rd/s;  $\beta$  is the sensibility coefficient at the impact velocity of the pulsation,  $\beta = 50703$ .

We can observe a fast increase of the pulsations during the passage from low to high impact velocities.

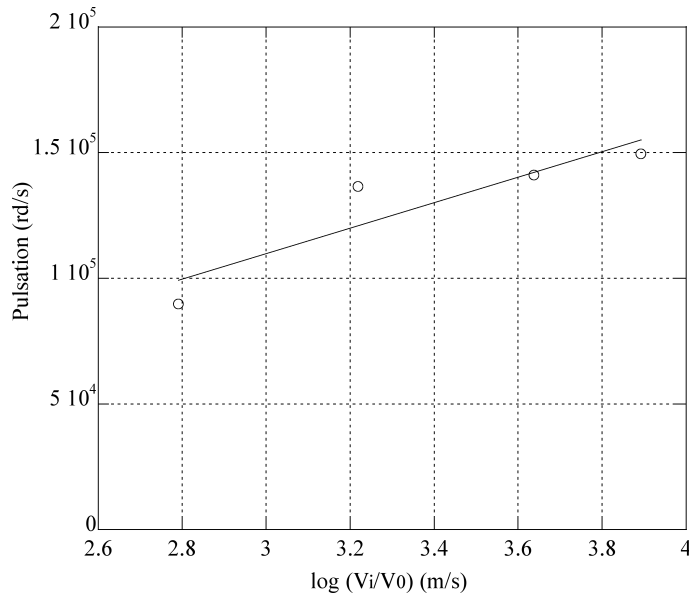


FIG. 11. Influence of the impact velocity on pulsation.

We will now take successively into consideration the effects of bending moment, shear force, rotational inertia and cantilever shape. Table 3 collects all results of the theoretical calculations using the method of Rayleigh [18, 19] (see Appendix 2 for details) which is based on the principle of the energy conservation. The correction of the specimen mass and of the stiffness are presented under the form of the ratios  $m_e/m_0$  and  $K/K_0$ , where  $K$  represents the rigidity of the specimen,  $m_0 = \rho.A.S$  corresponds to the mass between the specimen's supports,  $m_e = 17/35 m_0$  corresponds to the equivalent mass of the specimen calculated by G. WILLIAMS [20],  $K_0 = 48EI/S^3$  corresponds to the specimen stiffness.

**Table 3.** Theoretical determination of the first resonant frequencies.

Conditions	$K/K_0$	$K$ [ $10^6$ N/m]	$m_e/m_0$	$m_e$ [g]	$m_1 + m_e$ [kg]	$\omega$ [rd/s]
Bending moment	1.000	2.4	0.486	3.210	0.218200	3316
Moment + cantilever	0.883	2.12	0.521	3.440	0.218440	3122
Moment + shearing	0.917	2.2	0.471	3.113	0.218113	3175
Moment + shearing + rotational inertia	0.917	2.2	0.554	3.656	0.218656	3174

In order to reduce experimentally the amplitude and pulsations values, we have performed the spring-back tests for the fibre-glass-reinforced PA6 specimen.

Figure 12 shows the evolution of the force as a function of displacement for this type of test. The return to the initial position explains a restitution of a part of the energy of the specimen which is stored in the projectile which springs back at the final velocity  $V_f$ . The force component which represents the first frequency can be described as following:

$$(3.5) \quad F(t) = A_1/\omega_1 \sin(\omega_1 t),$$

where  $A_1$  represents the amplitude of this mode.

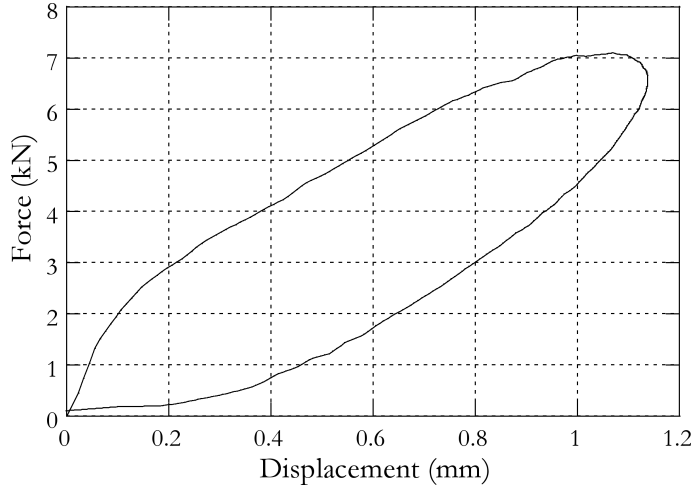


FIG. 12. Spring-back test for fibre-glass-reinforced PA6 specimen, initial impact velocity of  $V_i = 7.4$  m/s.

We have a similar relation for the displacement:

$$(3.6) \quad x(t) = B_1/\omega_1 \sin(\omega_1 t).$$

As a consequence, the values of the amplitudes and pulsations have been determined numerically using the method of least squares. The values of these parameters are reported in Table 4.

**Table 4.** Calculation of the amplitude and pulsation for the spring-back test of the fibre-glass-reinforced PA6 specimen.

Impact velocity [m/s]	$F$ [N]	$x$ [mm]
7.4	$A_1 = 2.9 \cdot 10^7 \pm 5.3 \cdot 10^5$	$B_1 = 4630.1 \pm 27$
	$\omega_1 = 4479.3 \pm 28$ rd/s	$\omega_1 = 4178.2 \pm 8.83$ rd/s

The mean pulsation values are:  $4479.3 \pm 27.63$  rd/s for the force and  $4178.2 \pm 8.83$  rd/s for the displacement. These values represent relative differences of 26% and 20%, respectively, compared to the pulsations given by the method of Rayleigh. This dispersion can be explained by the presence of the second mode oscillations (high impact velocities) which are originated from the acceleration field.

#### 3.4. Influence of the acceleration field

It is important to analyze the impact of the acceleration field in the specimen under dynamic loading. In order to do so, the specimen will be modelled as the 3-point bending configuration by the mass-spring system (Fig. 13).

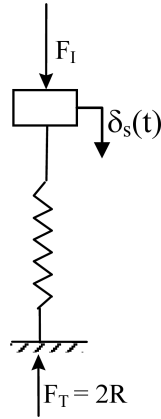


FIG. 13. Schema used for inertia correction.

The sum of the support reactions measured at the level of the output bar is  $2R = F_T$ , whereas  $F_I$  is the force applied at the impact point at the specimen. Therefore, the fundamental law of the dynamic described for the specimen receives the following form:

$$(3.7) \quad F_I(t) - F_T(t) = m_e \ddot{\delta}_s(t),$$

where  $m_e$  is a reduced mass of the specimen defined here above and  $\delta_s(t)$  represents a deflection measured at the centre of the specimen defined by the Eq. (2.4). The initial conditions of  $\delta(\tau) = \delta(t) = 0$ , at  $t = 0$ .

When no acceleration is present such as in the quasi-static mode,  $F_I$  is equal to  $F_T$ . However, under dynamic conditions, we shall introduce the factor of dynamic correction  $\gamma$ , defined by the following formula:

$$(3.8) \quad \gamma(t) = \frac{F_T(t)}{F_I(t)}.$$

The factor of dynamic correction will also be given by:

$$(3.9) \quad \gamma(t) = \frac{F_I(t) - m_e \ddot{\delta}_s(t)}{F_I(t)}$$

or:

$$(3.10) \quad \gamma(t) = \frac{F_T(t)}{F_T(t) + m_e \ddot{\delta}_s(t)}.$$

This correction factor allows to illustrate the field of acceleration of the force applied at the central point of the specimen. In case of our configuration, the field of acceleration is deduced from the field of displacement measured at the central point of the specimen. The example of this correction is presented in Fig. 14 as a function of time. It can be observed the dynamic effects are more important when the specimen is in one point bending (loss of contact between the specimen and the supports). The correction factor itself increases at higher impact velocities (Fig. 15). The value  $\gamma = 1$  corresponds to the quasi-static loading. Therefore any deviations reflect the influence of the field of acceleration in the dynamic case.

The sum of the support reactions are calculated experimentally by the transmitted force. If the inertial component is known, the applied force at the impact point of the specimen is determined through the Eq. (3.11) without any need to define the stiffness:

$$(3.11) \quad F_I = m_e \ddot{\delta}_{\text{ext}}(t) + \left( \frac{\pi}{4} (D_{\text{ext}}^2 - D_{\text{int}}^2) E_{\text{tub}} - m_e C_0 \right) \dot{\epsilon}_T(t).$$

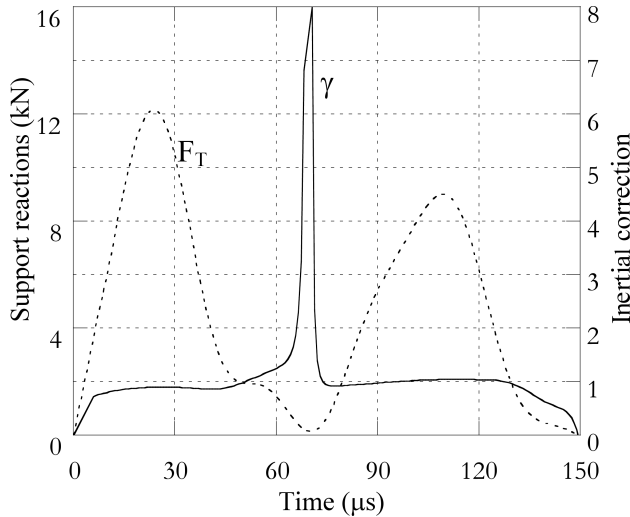


FIG. 14. Dynamic correction for the impact velocity of  $V_i = 25$  m/s.

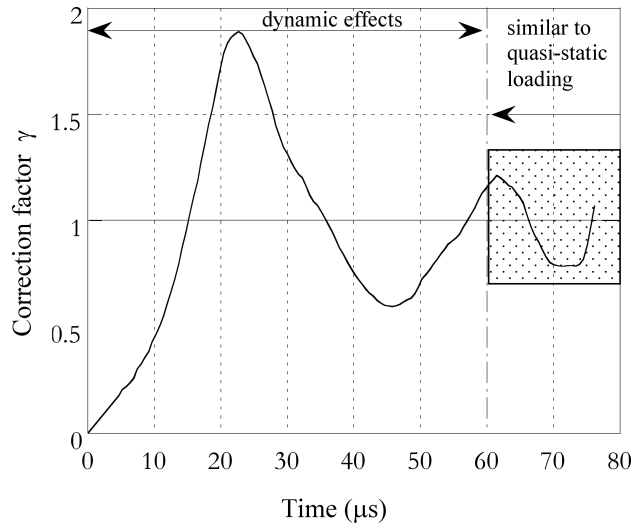


FIG. 15. Dynamic correction for the impact velocity of  $V_i = 58$  m/s.

Figure 16 presents the evolution in time of the applied force for different impact velocities.

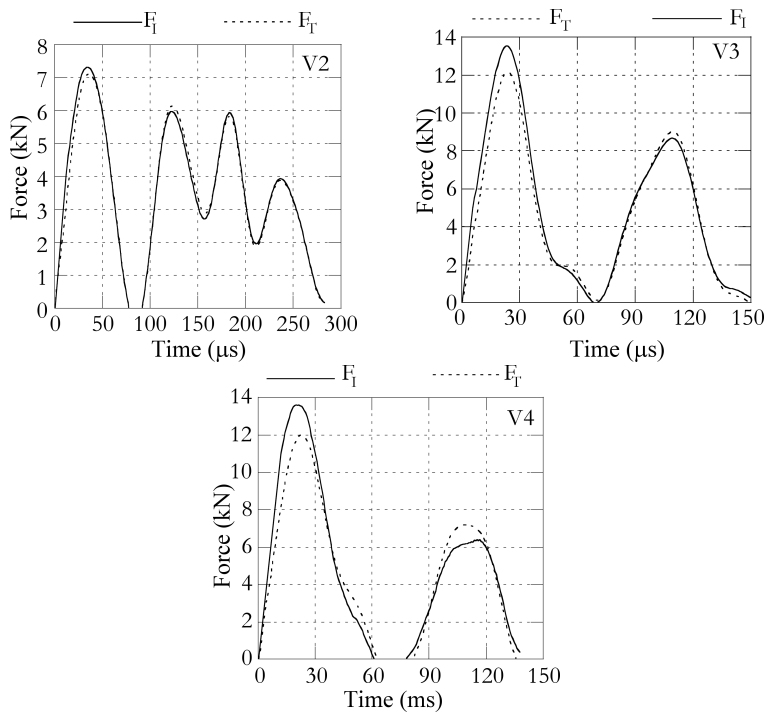


FIG. 16. Comparison of the force obtained on the impact point and close to the support  $V_2 = 18.27$  m/s,  $V_3 = 25$  m/s,  $V_4 = 38$  m/s.

Before the contact is lost between the specimen and the supports, a comparison of two forces ( $F_I > F_T$ ) shows a good reproducibility of the model. On the other hand, when the contact is re-established, we can see in Fig. 16 that the amplitude of the force  $F_I$  is slightly inferior than the amplitude of the force  $F_T$ , because the adopted model does not take into consideration the delay which exists between the beginning of these two loads ( $F_I$  and  $F_T$ ). Moreover, this time shift can be influenced by the dispersion of the bending waves at the specimen boundaries as well as by the arrival of the first transversal wave at the rupture point.

Figure 17 presents the evolution of shock time as a function of the impact velocity. We can observe that the shock time diminishes with the impact velocity because the rupture load is reached faster.

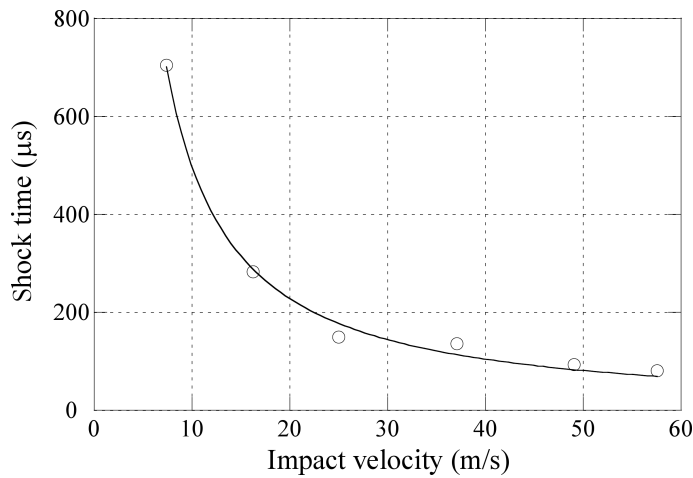


FIG. 17. Influence of impact velocity on the shock time.

#### 4. CONCLUSION

In order to study the behaviour of the glass-fibre-reinforced Polyamid 6 in dynamic conditions, we have elaborated a system to limit disturbances appearing at low frequencies during the tests. This made us possible to better describe oscillations amplitudes at the force-time curve. It should be noted that this is not the case for the typical Charpy test during which important parasite oscillations are measured due to hammer vibrations and not due to the force applied at the specimen.

This new technique allows to measure in a fast way not only the force at the supports, but also the displacement at the specimen centre at high impact velocities.

## APPENDIX A. FLEXURAL RESPONSE OF A SEMI-INFINITE BEAM

In case of a simply supported beam, loaded in the 3-point bending configuration, free unamortized vibrations are governed by the following equation where only a bending moment is taken into account:

$$(A.1) \quad EI \frac{\partial^4 Y(z, t)}{\partial z^4} + \rho A \frac{\partial^2 Y(z, t)}{\partial t^2} = 0,$$

where  $E$  is the Young's modulus of the material,  $\rho$  is its volume mass;  $I$  and  $A$  are respectively the quadratic moment  $I = \frac{BW^3}{12}$  and the specimen cross-section  $A = BW$ .

We assume  $Y(z, t)$  can be written in a separable form:  $Y(z, t) = y(z)f(t)$ , then we divide it by the term  $EI$  in order to receive:

$$(A.2) \quad \frac{y^{IV}(z)}{y(z)} + \frac{\rho A}{EI} \frac{f''(t)}{f(t)} = 0,$$

where  $y^{IV}(z)$  and  $f''(t)$  represent respectively the fourth derived of  $y(z)$  with respect to  $z$  and the second derived of  $f(t)$  with respect to time. Again, we divide by  $y^{IV}(z)f(t)$  in order to separate the variables:

$$(A.3) \quad y^{IV}(z)f(t) + \frac{\rho A}{EI} y(z)f''(t) = 0.$$

As the first term of the Eq. (A.3) is only a function of  $z$  and the second one only depends on  $t$ , the equation cannot be satisfied for any value of  $z$  or  $t$  unless both terms become the constant value  $C$ .

$$(A.4) \quad \frac{y^{IV}(z)}{y(z)} = -\frac{\rho A}{EI} \frac{f''(t)}{f(t)} = C = k^4.$$

We assume  $C = k^4$  and we obtain two classical differential equations:

$$(A.5) \quad y^{IV}(z) - k^4 y(z) = 0,$$

$$(A.6) \quad f''(t) + \omega^2 f(t) = 0,$$

where

$$(A.7) \quad \omega^2 = k^4 \frac{EI}{\rho A}.$$

If  $f_0$  and  $f'_0$  are defined as initials conditions at  $t = 0$ , the general solution of the Eq. (A.6) is given in the following form:

$$(A.8) \quad f(t) = f_0 \cos \omega t + \frac{f'_0}{\omega} \sin \omega t.$$

While solving the first differential Eq. (A.5) in the form  $y(z) = e^{rz}$ , we show that  $y(z)$  is a combination of trigonometric and hyperbolic functions:

$$(A.9) \quad y(z) = A_1 \cos kz + A_2 \sin kz + A_3 \cosh kz + A_4 \sinh kz,$$

where the constant values  $A_i$  are determined by boundary conditions. At the abscissa points  $z = 0$  and  $z = S$ , the deformation and the moment are equal to zero:  $y(0) = y(S) = 0$  and  $EIy''(0) = EIy''(S) = 0$ .

Finally, we obtain  $A_1 = A_3 = A_4 = 0$  and the only condition is:  $A_2 \sin kz = 0$ . As  $A_2$  cannot be zero, we find that  $k = \frac{n\pi}{S}$  or  $n$  is the natural number. By replacing the expression of  $k$  in the Eq. (A.7), the pulsation of the proper mode of the specimen can finally be expressed:

$$(A.10) \quad \omega_n = n^2 \pi^2 \sqrt{\frac{EI}{\rho AS^4}} = n^2 \pi^2 \sqrt{\frac{EI}{m_0 S^3}}$$

$m_0 = \rho AS$  corresponds to the mass between the specimen supports.

## APPENDIX B. METHOD OF RAYLEIGH

### B.1. Bending moment only

$$\omega_1^2 = \frac{48EI}{S^3} \frac{1}{\left(m_1 + \frac{17}{35}m_0\right)},$$

$$m_e = \frac{17}{35}m_0.$$

### B.2. Shearing effect

$$\omega_1^2 = \frac{48EI}{S^3} \frac{1 + k' \frac{E}{G} \left(\frac{W}{S}\right)^2}{m_1 \left[1 + k' \frac{E}{G} \left(\frac{W}{S}\right)^2\right]^2 + (\mu_2 S) \left[\frac{17}{35} + \frac{4}{5} k' \frac{E}{G} \left(\frac{W}{S}\right)^2 + \frac{1}{3} \left(k' \frac{E}{G}\right)^2 \left(\frac{W}{S}\right)^4\right]},$$

$$m_e = \frac{17 (\mu_2 S) \left[1 + \frac{28}{17} k' \frac{E}{G} \left(\frac{W}{S}\right)^2 + \frac{35}{51} \left(k' \frac{E}{G}\right)^2 \left(\frac{W}{S}\right)^4\right]}{35 \left[1 + k' \frac{E}{G} \left(\frac{W}{S}\right)^2\right]^2},$$

$$K = \frac{48EI}{S^3} \frac{1}{\left[1 + k' \frac{E}{G} \left(\frac{W}{S}\right)^2\right]}.$$

*B.3. Effect of the inertial rotation*

$$\omega_1^2 = \frac{\frac{48EI}{S^3} \left(1 + k' \frac{E}{G} \left(\frac{W}{S}\right)^2\right)}{\left[m_1 \left(1 + k' \frac{E}{G} \left(\frac{W}{S}\right)^2\right)^2 + a^*\right]},$$

$$m_e = \frac{17}{35} (\mu_2 S) \frac{b^*}{\left[\left(1 + k' \frac{E}{G} \left(\frac{W}{S}\right)^2\right)^2\right]},$$

$$K = \frac{48EI}{S^3} \frac{1}{\left[1 + k' \frac{E}{G} \left(\frac{W}{S}\right)^2\right]},$$

where

$$a^* = (\mu_2 S) \left[ \frac{17}{35} + \frac{2}{5} \left(1 + 2k' \frac{E}{G}\right) \left(\frac{W}{S}\right)^2 + \frac{1}{3} \left(k' \frac{E}{G}\right) \left(2 + k' \frac{E}{G}\right) \left(\frac{W}{S}\right)^4 + \frac{1}{3} \left(k' \frac{E}{G}\right)^2 \left(\frac{W}{S}\right)^6 \right],$$

$$b^* = \left[ 1 + \frac{14}{17} k' \frac{E}{G} \left(1 + 2k' \frac{E}{G}\right) \left(\frac{W}{S}\right)^2 + \frac{35}{51} \left(k' \frac{E}{G}\right) \left(2 + k' \frac{E}{G}\right) \left(\frac{W}{S}\right)^4 + \frac{35}{51} \left(k' \frac{E}{G}\right)^2 \left(\frac{W}{S}\right)^6 \right].$$

*B.4. Taking into account the cantilever of the specimen*

$$\omega_1^2 = \frac{\frac{48EI}{S^3} \left[1 + 8p^3 + k' \frac{E}{G} (1 + 2p) \left(\frac{W}{S}\right)^2\right]}{m_1 \left[1 + 8p^3 + k' \frac{E}{G} (1 + 2p) \left(\frac{W}{S}\right)^2\right]^2 + c^*},$$

$$m_e = \frac{17}{35} (\mu_2 S) \frac{1 + \frac{210}{17} p^3 - \frac{336}{17} p^5 + \frac{160}{17} p^7 + \frac{70}{17} \left[C_1 \left(\frac{W}{S}\right)^2 + C_2 \left(\frac{W}{S}\right)^4 + C_3 \left(\frac{W}{S}\right)^6\right]}{\left[1 + 8p^3 + k' \frac{E}{G} (1 + 2p) \left(\frac{W}{S}\right)^2\right]^2},$$

$$K = \frac{48EI}{S^3} \frac{1}{\left[1 + 8p^3 + k' \frac{E}{G} (1 + 2p) \left(\frac{W}{S}\right)^2\right]},$$

where

$$c^* = (\mu_2 S) \left\{ \frac{17}{35} + 3p^3 - \frac{48}{5}p^5 + \frac{32}{7}p^7 + 2 \left[ C_1 \left( \frac{W}{S} \right)^2 + C_2 \left( \frac{W}{S} \right)^4 + C_3 \left( \frac{W}{S} \right)^6 \right] \right\},$$

and  $G$  is the Coulomb modulus and  $p$  is the value of cantilever.

#### ACKNOWLEDGMENT

The authors express their gratitude to Prof. J.R. Klepaczko for his knowledge and his teaching in the field of dynamic behaviour, fracture and the technique related to Hopkinson bar technique.

#### REFERENCES

1. JIANG F., VECCHIO K.S., *Hopkinson Bar Loaded Fracture Experimental Technique: A Critical Review of Dynamic Fracture Toughness Tests*, Appl. Mech. Rev., **62**, 060802, 2009.
2. CHARPY G., *Note sur l'essai des métaux à la flexion par choc de barreaux entaillés*, Mémoire et compte-rendus de la Société des ingénieurs civils de France, 1901.
3. FAZAL A., KEVIN S., *Viscoelastically prestressed polymeric matrix composites – Effects of test span and fibre volume fraction on Charpy impact characteristics*, Composites, **44**, 472–479, 2013.
4. HOPKINSON B., *A method of measuring the pressure produced in the detonation of explosives or by impact of bullet*, Phil. Trans, **213**, 437, 1914.
5. NICHOLAS T., *Notched bend behavior of beryllium over a wide range of strain rates*, Technical Report AFML-TR-75-177, Wright-Patterson AFB, Ohio, 1975.
6. RUIZ C., MINES R.A., *The Hopkinson pressure bar: an alternative to the instrumented pendulum for Charpy tests*, Int. J. Fracture., **29**, 101, 1985.
7. YOKOYAMA T., KISHIDA K., *A novel impact three-point bend test method for determining dynamic fracture-initiation toughness*, Exp. Mech., **29**, 188, 1989.
8. TANAKA K., KAGATSUME T., *Impact bending test on steel at low temperatures*, Bull. JSME., **23**, 1736, 1980.
9. FENGCHUN J., KENNETH S.V., *Hopkinson Bar Loaded Fracture Experimental Technique: A Critical Review of Dynamic Fracture Toughness Tests*, Appl. Mech. Rev., **62**, 6, 2009.
10. DELVARE F., HANUS J.L., BAILLY P., *A non-equilibrium approach to processing Hopkinson Bar bending test data: Application to quasi-brittle materials*, International Journal of Impact Engineering, **37**, 1170–1179, 2010.
11. GOVENDER R.A., LANGDON G.S., NURICK G.N., CLOETE T.J., *Impact delamination testing of fibre reinforced polymers using Hopkinson Pressure Bars*, Engineering Fracture Mechanics, **101**, 80–90, 2013.

12. NAZARENKO E., *Comportement à rupture d'un composite à fibres céramiques et matrice vitrocéramique sous sollicitations statiques et dynamiques*, Thèse de l'Ecole Centrale de Paris, 1992.
13. HANUS J.L., MAGNAIN B., DURAND B., RODRIGUEZA J., BAILLY P., *Processing dynamic split Hopkinson three-point bending test with normalized specimen of quasi-brittle material*, *Mechanics & Industry*, **13**, 06, 381–393, 2012.
14. ZHAO H., *Analyse de l'essai aux barres d'Hopkinson. Application à la mesure du comportement dynamique des matériaux*, Thèse de l'ENPC et de l'Ecole Polytechnique, 1992.
15. KLEPACZKO J.R., *An experimental technique for shear testing at high and very high strain rates. The case of mild steel*, *Int. J. Impact. Engng.*, **15**, 25, 1994.
16. KLEPACZKO J.R., MATYSIAK S.J., *Analysis of longitudinal impact on semi-infinite circular bars and tubes*, Appendix No. 2, The Final Technical Report Contract DAJA 45-90-C-0052, Metz, October, 1992.
17. NFEN 10045-1, *Essai de flexion par choc sur éprouvettes entaillées*, Méthodes d'essais, Partie I, Octobre, 1992.
18. LORRIOT L., *Charpy impact test analysis. Dynamic behaviour of a 2D-carbon/carbon composite material*, Thesis of university Bordeaux, 1996.
19. CLOUGH R.W., PENZIEN J., *Dynamique des structures*, Tome I, Editions PLURALIS, 1980.
20. WILLIAMS J.G., *The analysis of instrumented impact tests using a mass spring model*, *International Journal of Fracture*, **33**, 209, 1987.

*Received May 6, 2014; revised version October 29, 2014.*

---